Obtaining and Evaluation of Synthesis Gases from Biomass Gasification using Finite Element Analysis

FABREGAS, J.[A], FONTALVO, C.E.[A], VALENCIA, G.E.[B*], OBREGON, L.G [B], CARDENAS, Y.D [C]

[a]*Universidad Autónoma del Caribe, Colombia*

[b]*Universidad del Atlántico, Colombia*

[c]*Universidad de la Costa, Colombia*

**Guillermo Eliecer Valencia Ochoa, guillermoevalencia@mail.uniatlantico.edu.co*

Abstract

Given the need to implement non-conventional sources for the generation of energy, it is necessary to characterize the natural or residual agro-industrial resources that can be used for the conversion of energy. In this work, a study is carried out to obtain the synthesis gas produced in a bioreactor using the gasification of biomass, such as pinewood, rice husk, coconut husk and palm shell, to analyze its potential as synthesis gas. This gas is obtained using a finite element software for the parameterization of the relevant models for the calculation of its production by biomass gasification through its final composition and the chemical analysis obtained from studies carried out on the physicochemical properties of biomass. As a result, the CO and H_2 production components are obtained for each biomass sample, evaluated at 1020K. These results are similar to those obtained by experimental designs, showing that using computational techniques a good approximation is received from the analysis of residual material for use as fuel.

Keywords: synthesis gases, Biomass Gasification, finite element.

1. Introduction

In the agricultural sector, crop products and residues are currently used as sources of energy generation from their use as a fuel, which can be obtained from biomass by thermochemical conversion or biochemical conversion. To make good use of the biomass's energy potential, its components must be characterized by the ultimate and proximate analysis, which indicates the fixed carbon content, volatile material, and moisture content. It is therefore advisable to perform gasification operations to obtain the production of synthesis gas present in crop product residues [1].
On the other hand, process simulators, such as ASPEN PLUS are widely used to study conversion processes that involve biomass to evaluate the performance, emissions, and costs of gasification plants, the integrated combined cycle and gasification systems. Many studies about gasification have been done, such as methanol synthesis [2], indirect coal liquefaction processes [3], integrated combined cycle power and gasification plants [4], atmospheric combustion processes in fluidized bed reactors [5], fluidized bed coal gasifiers [6], coal hydrogasification processes [7], and coal gasification [8]. However, it was found that the work aimed at studying biomass gasification is limited.

The Computational Fluid Dynamics (CFD) using a validated gasification model have been used to examine the effect of biomass quantity on a biomass co-production process. The model was validated with actual operating data from an integrated gasification combined cycle plant located in Spain [9], where the results showed that the concentration of CO decreases and the concentration of H_2 increases when the mixing ratio increases. Also, new mathematical tools have been implemented to downstream fixed bed gasifier using biomass material such as neural network and fuzzy logic to predict the behavior of the operation unit [10], [11]. In their results, they show that the control system makes it possible to establish synthesis gas production analyses by controlling the temperature in the injection area.

Regarding biomass characterization, a comparative study of the central physicochemical properties of rice husk biomass was done. The research was carried out at the universities of Canada, California, China PR and Ibague Colombia. The results showed that there is a similarity between the physicochemical characteristics of the biomass studied from the mentioned regions and those obtained when the oxidation temperature reached around 1200K [12].

A three-phase flow model, together with a thermal equilibrium model to study the operation of downstream biomass gasifiers was also developed, and complemented with some gasification experiments to obtain pyrolysis kinetics. Then, a CFD modeling was established to predict the synthesis gas composition and temperature, respectively [13].

The performance of a CFD modeling of biomass gasification was evaluated using the finite velocity and eddy dissipation model by solving the three dimensional Navier-Stokes equations in a stationary state with the Eulerian-Lagrangian method with gas-phase chemical reactions. It lets to solve the carbonization gasification reactions, using the random pore model with bulk diffusion effects [9].

Many results obtained in the CFD software are reasonable regarding molar fractions of the species presented and the temperature at the exit of the system compared to the operating data, but they cannot be used for any biomass. Therefore, in this study the gasification process of biomass with descending flow is carried out using CFD analysis, evaluating the composition of the synthesis gases resulting from gasification of pine wood, rice husk, coconut husk, and palm kernel Cusco.

2. Methodology

2.1 Synthesis gas production from biomass gasification

The gasification operation involves obtaining a synthesis gas from a solid or liquid organic material through partial oxidation composed mainly of hydrogen (H_2) and carbon monoxide (CO), carbon dioxide (CO_2), water (H_2O), methane (CH_4), heavy hydrocarbons (C_{2+}), and nitrogen (N_2) [14]. In this process, the reactions are carried out at temperatures between 500 °C and 1400 °C and pressures ranging from atmospheric values to high pressures around 30 bar, where the oxidizing agent used are air, pure oxygen, steam or mixtures of them [15]. Gasifiers using air produce gas with high nitrogen concentrations and a low energy value of 4 to 6 MJ/m^3. Gasifiers using oxygen and steam as an oxidizer produce a synthesis gas containing high concentrations of hydrogen and carbon monoxide with calorific values between 10 and 20 MJ/m^3.

2.2 Biomass physicochemical characteristics

The biomasses studied present physicochemical characteristics that give a good performance as a combustible material. Table 1 shows the results of the proximate and ultimate analysis of the samples of pine wood, rice husk, coconut husk, and palm kernel.

The gasification system is a down-flow system which enters the biomass through the upper opening and injects high-temperature air from one side into a reduction section, and finally an outlet pipe above the ash accumulation tank. Fig. 1 shows the gasification system indicating the zones.

Table 1. Proximate and ultimate analysis

Proximate Analysis				
	Pinewood	**Rice Husk**	**Coconut Husk**	**Palm Shells**
Volatile	0,6750	0,6233	0,7145	0,7274
Fixed Carbon	0,2241	0,1587	0,1528	0,1687
Ash	0,0269	0,1703	0,0126	0,0247
Moisture	0,0741	0,0476	0,1201	0,0792
Ultimate Analysis				
	Pinewood	**Rice Husk**	**Coconut Husk**	**Palm Shells**
C	0,5437	0,4980	0,4540	0,4860
H	0,0647	0,0700	0,0905	0,0999
O	0,3862	0,4240	0,4537	0,4047
N	0,0051	0,0020	0,0016	0,0086
S	0,0002	0,0060	0,0003	0,0007

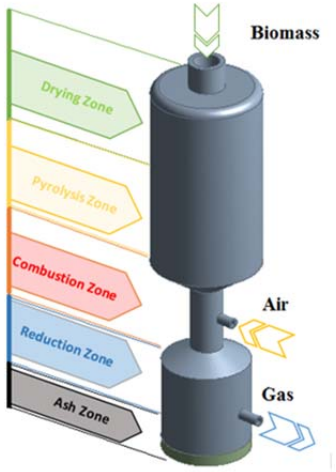

Fig. 1. Gasification system

The heterogeneous and homogeneous reactions that define the gasification process are shown in Table 2. Also, complete and incomplete combustion reactions are considered, methanation reactions, carbon monocyte oxidation, oxidation of hydrogen, methane oxidation and water - water reactions that describe the system[16].

Table 2. Gasification reactions

Heterogeneous oxidation
$C + O_2 \rightarrow CO_2 \ -394\frac{MJ}{kmol}$
$C + \frac{1}{2}O_2 \rightarrow CO \ -111\frac{MJ}{kmol}$
Homogeneous oxidation
$CO + \frac{1}{2}O_2 \leftrightarrow CO_2 \ -283\ \frac{MJ}{kmol}$
$CO + 3H_2 \rightarrow CH_4 + H_2O \ -206\ \frac{MJ}{kmol}$
$H_2 + \frac{1}{2}O_2 \rightarrow H_2O \ -242\ \frac{MJ}{kmol}$
$CH_4 + \frac{3}{2}O_2 \rightarrow CO + 2H_2O \ -519\ \frac{MJ}{kmol}$
Heterogeneous reactions in equilibrium

$C + CO_2 \rightarrow 2CO \ + 172 \frac{MJ}{kmol}$ $C + H_2O \rightarrow CO \ + H_2 + 131 \frac{MJ}{kmol}$ $C + 2H_2 \rightarrow CH_4 \ - 72 \frac{MJ}{kmol}$
Heterogeneous reactions in equilibrium
$C + CO_2 \rightarrow 2CO \ + 172 \frac{MJ}{kmol}$ $C + H_2O \rightarrow CO \ + H_2 + 131 \frac{MJ}{kmol}$ $C + 2H_2 \rightarrow CH_4 \ - 72 \frac{MJ}{kmol}$
Homogeneous reactions in equilibrium
$CO + H_2O \leftrightarrow CO_2 + H_2 \ - 41 \ \frac{MJ}{kmol}$ $CH_4 + H_2O \rightarrow CO + 3H_2 \ - 206 \ \frac{MJ}{kmol}$

Gasification involves a series of endothermic reactions, stimulated by the heat produced in the combustion reactions described above, which transform biomass into a combustible gas. The four most important endothermic reactions are:

- Water-gas reaction, where partial oxidation of coal with steam from possible sources such as moisture from the supplied air, evaporation of moisture from the solid fuel, decomposition of biomass or steam supplied to the gasifier with air or oxygen occurs.
- CO_2 reduction, where the CO_2 present in the gasifier can react with the carbon to produce CO
- Water-gas shift reaction, where the reduction of steam by carbon monoxide is highly desirable due to hydrogen production.
- Methane reaction, where methane (CH_4) can be produced in the gasifier, which can be accelerated by nickel-based catalysts at temperatures of 1100 °C and pressures between 6 and 8 bar.

Finally, the composition of the gas obtained by gasification depends on certain parameters such as biomass composition, gasification medium, pressure, temperature, the moisture content of solids, and the type of gasifier [17], [18].

2.1 Computational model

For the development of the mathematical model using CFD analysis, it is necessary to use tools that allow the study of fluid flow behavior represented by the K-epsilon turbulence mode K-epsilon (k-ε) shown in equations (1-3), [9].

$$\frac{\partial}{\partial t}(\rho k) + \frac{\partial}{\partial x_j}(\rho k u_j) = \frac{\partial}{\partial x_j}\left[\left(\mu + \frac{\mu_t}{\partial_k}\right)\frac{\partial k}{\partial x_j}\right] + G_k + G_b - \rho\varepsilon - Y_M + S_k \quad (1)$$

$$\frac{\partial}{\partial t}(\rho\varepsilon) + \frac{\partial}{\partial x_j}(\rho k u_j) = \frac{\partial}{\partial x_j}\left[\left(\mu + \frac{\mu_t}{\sigma_\varepsilon}\right)\frac{\partial s}{\partial_j}\right] + \rho C_1 S\varepsilon - \rho C_2 \frac{\varepsilon^2}{k + \sqrt{v\varepsilon}} + C_{1\varepsilon}\frac{\varepsilon}{k}C_{3\varepsilon}G_b + S_\varepsilon \quad (2)$$

$$C_1 = max\left[0.43, \frac{n}{n+5}\right], n = S\frac{k}{\varepsilon}, S = \sqrt{2S_{ij}S_{ij}} \quad (3)$$

Where G_k is the turbulence generation of kinetic energy due to average velocity gradients, G_b is the generation of turbulent kinetic energy due to buoyancy, Y_M represents the contribution of fluctuating expansion incompressible turbulence to the overall dissipation rate.

The energy conservation models represented by the equation (4) are activated.

$$\frac{\partial}{\partial t}\rho E + \nabla \cdot (\rho \bar{v}_r H + p\bar{u}_r) = \nabla \cdot (k\nabla T + \bar{\bar{\tau}} \cdot \bar{v}) + S_h \quad (4)$$

Where ρ is the density, E is the total energy, H is the total enthalpy, $\bar{v}_r$ and $\bar{u}_r$ are radial velocities. The conservation models of species is shown in equation (5).

$$\frac{\partial}{\partial t}\rho Y_i + \nabla \cdot (\rho \bar{v} Y_i) = -\nabla \cdot \bar{J}_i + R_i + S_i \quad (5)$$

Where R_i is the net rate of production of species I by chemical reaction, S_i is the rate of scattered phase addition creation plus any user-defined source, $\bar{J}_i$ is the flow of diffusion of species i and Y_i is the mass fraction per species i.

Using the Arrhenius expression, the reaction rate is calculated as follows, see equation (6), where A is an exponential pre-factor, T is the process temperature, β is an exponent of temperature, E is the activation energy for the reactions, and R is the universal constant of gases.

$$k = AT^{\beta} e^{\frac{-E}{RT}} \quad (6)$$

An alternative method is the use of the non-mixed model for liquid fuel or coal combustion which can use the non-mixed model if the simulation includes carbon particles. In this case, the fuel enters to the gas phase within the computational domain at speed determined by the laws of evaporation, devolatilization, and combustion of coal that govern the dispersed phase.

The mean mixture fraction is calculate as equation (7), where the term S_m is due solely to transfer of mass into the gas phasefrom liquid fuel droplets or reacting particles, $\bar{f}$ is mixture fraction, σ_t is a constant and μ_t is the subgrid-scale viscosity.

$$\frac{\partial}{\partial t}\left(\rho \bar{f}\right) + \nabla \cdot \left(\rho \bar{v} \bar{f}\right) = \nabla \cdot \left(\frac{\mu_t}{\sigma_t} \nabla \bar{f}\right) + S_m$$
(7)

The instantaneous enthalpy for the fractions of the mixture is estimate as equation (8).

$$H' = \sum_j m_j H_j = \sum_j m_j \left[\int_{T_{ref,j}}^{T} C_{p,j} dT + h_j^0(T_{ref,j})\right]$$
(8)

The time-averaged values of species mole fractions and temperature are computed as equation (9), where the probability density function $p(f)$, describing the temporal fluctuations of f in the turbulent flow, φ_i is the equivalence ratio.

$$\overline{\varphi_i} = \int_0^1 \varphi_i(f, \overline{H'})\, p(f)\, df$$
(9)

Therefore, the modeled transport equation for time-averaged enthalpy is estimate as equation (10), where S_h account for term due to radiation, heat transfer to wall boundaries, and heat exchange.

$$\frac{\partial}{\partial t}(\rho \overline{H'}) + \nabla \cdot \left(\rho \bar{\bar{v}} \overline{\overline{H'}}\right) = \nabla \cdot \left(\frac{k_t}{C_p} \nabla \overline{f\overline{H'}}\right) + S_h$$
(10)

2.2 Process parameters and boundary conditions

From the calculation procedure, the CFD program creates for each biomass an empirical molecule with its lower calorific value. Next, the decomposition of each biomass is represented into a volatile material fraction, fuel material fraction, and ash fraction as shown in Table 3.

Table 3. Gasification reactions, [19].

Pinewood
$Biomass_{pinewood} \rightarrow 0{,}729\ Vol_{pinewood} + 0{,}242\ Char + 0{,}029\ Ash$ $Vol_{pinewood} = C0{,}97\ H2{,}56\ O0{,}96\ N0{,}0146$ $Biomass_{pinewood} = LCV\ of\ 20292{,}976\ KJ/kg$
Rice husk
$Biomass_{rice\ husk} \rightarrow 0{,}654\ Vol_{rice\ husk} + 0{,}166\ Char + 0{,}18 Ash$ $Vol_{rice\ husk} = C0{,}93\ H2{,}62\ O1{,}00\ N0{,}0054$ $Biomass_{rice\ husk} = LCV\ of\ 26544{,}133\ KJ/kg$
Coconut husk
$Biomass_{coconut\ husk} \rightarrow 0{,}812\ Vol_{coconut\ husk} + 0{,}173\ Char + 0{,}008 Ash$ $Vol_{coconut\ husk} = C0{,}84\ H3{,}26\ O1{,}03\ N0{,}0042$ $Biomass_{coconut\ husk} = LCV\ of\ 23976{,}558\ KJ/kg$
Palm Shells
$Biomass_{palm\ shells} \rightarrow 0{,}789\ Vol_{palm\ shells} + 0{,}183\ Char + 0{,}028 Ash$ $Vol_{palm\ shells} = C0{,}91\ H3{,}66\ O0{,}93\ N0{,}0227$ $Biomass_{palm\ shells} = LCV\ of\ 22654{,}986\ KJ/kg$

Regarding the boundary conditions, the air inlet velocity of the gasifier was configured so that the biomasses had the same generation temperature of synthesis gases of reference, 1020K. The air inlet pipe has a diameter of 1 inch, and the velocity was regulated in the range from 0,01 m/s to 0,05 m/s.

3. Results

The biomass composition in the gasification system is shown in Fig. 2. It can be seen that the biomass is located in high percentage in the upper part of the system (red color). The bottom practically does not contain biomass meaning that it has reacted completely with the hot combustion gases through an incomplete combustion producing CO_2, CO, CH_4, and H_2.

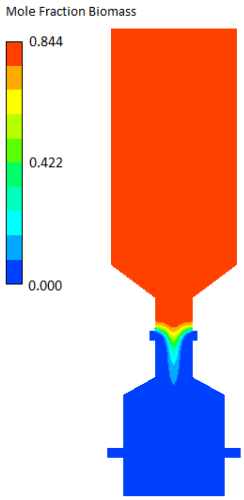

Fig. 2. Mole fraction biomass profile in the gasification system

The compositions of the synthesis gases for the biomass samples were obtained. The components CO_2, CO, CH_4, and H_2 for pinewood using a contour profile inside the gasifier are shown in Fig. 3, where the contours are similar between the biomass and the samples studied.

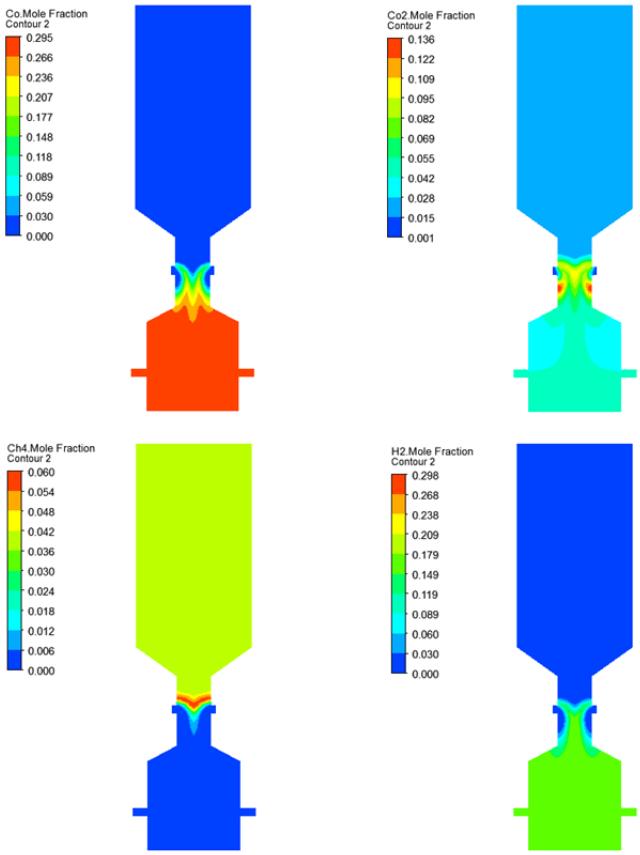

Fig. 3. CO_2, CO, CH_4 and H_2 percentage

The previous results shows the stages of production of the components of the synthesis gases inside the gasification system, with the CO and H_2 content being the highest percentage of production in the pinewood gasification process. Similar results were obtained with experimental measurements by. The temperature distribution and velocity field are shown in Fig. 4. It is observed that in the throat of the gasifier corresponding to the combustion zone, the highest temperature is reached. This temperature ranges from 700K to 1200K, and the velocity profiles reach a maximum of 0.105 m/s.

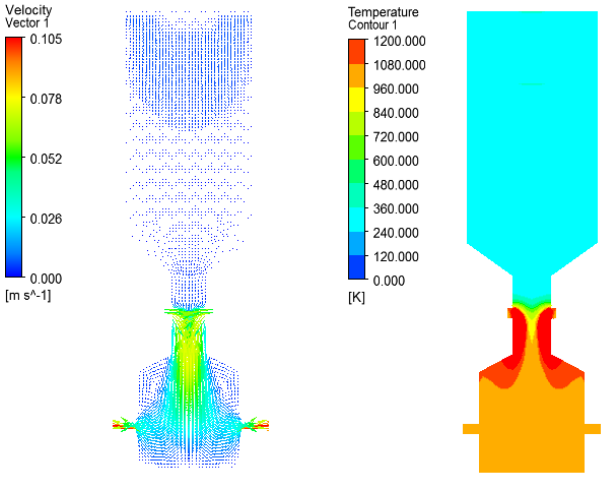

Fig. 4. Temperature and velocity profiles in the gasification system

The results of the components produced in the synthesis gases were grouped for each biomass and then tabulated for easy reading and comparison. The results of the formulations are shown in Fig. 5, where the biomasses with the most significant CO production in their gasification are pine wood and rice husk, while the biomasses with the most critical balance in CO and H_2 output are coconut husk and palm kernel.

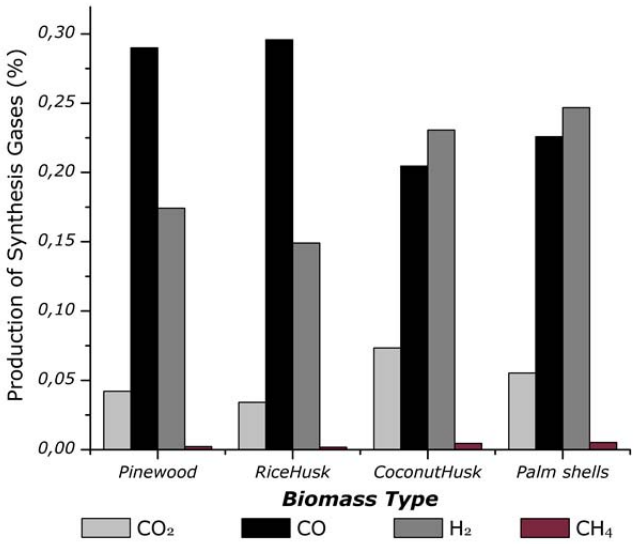

Fig. 5. Production of synthesis gases for biomass samples

4. Conclusions

It can be seen that modeling using CFD techniques allows a reasonable approximation of the results of synthesis gas production for biological material if the physicochemical characteristics such as proximate and ultimate analyses of the samples are known.

Rice husk presented the largest calorific value between samples, 26544.133 kJ/kg, followed by coconut husk with a value of 23976.558 kJ/kg, palm kernel with 22654.986 kJ/kg, and finally pine wood with 20292.976 kJ/kg. The rice husk is the material with the largest production since it is the residue of cereal most commercialized worldwide that can be used as a fuel because of its composition. It produces a high amount of CO followed by H_2.

Coconut husk and palm kernel in their results show a better balance between CO and H_2 production, with higher CH_4 output than rice husk and pine wood. The biomasses studied show their potential to produce synthesis gases by demonstrating that their highest CO production followed by H_2.

5. Reference

[1] L. G. Sequeda-Castañeda, A. R. Barrera-Bugallo, C. Celis, J. Iglesias, and L. Morales, "Evaluation of antioxidant and cytotoxic activity of extracts from fruits in fibroblastoma HT1080 cell lines: Four fruits with commercial potential in Colombia," *Emirates J. Food Agric.*, vol. 28, no. 2, pp. 143–151, 2016.

[2] R. O. dos Santos, L. de S. Santos, and D. M. Prata, "Simulation and optimization of a methanol synthesis process from different biogas sources," *J. Clean. Prod.*, vol. 186, pp. 821–830, Jun. 2018.

[3] L. Zhou, M. Duan, and Y. Yu, "Exergy and economic analyses of indirect coal-to-liquid technology coupling carbon capture and storage," *J. Clean. Prod.*, vol. 174, pp. 87–95, Feb. 2018.

[4] J. N. Phillips, M. R. Erbes, and R. H. Eustis, "Study of the Off-Design Performance of Integrated Coal Gasification Combined-Cycle Power Plants.," *Am. Soc. Mech. Eng. Adv. Energy Syst. Div. AES*, vol. 2–2, no. February, 1986.

[5] P. L. Douglas and B. E. Young, "Modelling and simulation of an AFBC steam heating plant using ASPEN/SP," *Fuel*, vol. 70, no. 2, pp. 145–154, Feb. 1991.

[6] P. Kaushal and R. Tyagi, "Advanced simulation of biomass gasification in a fluidized bed reactor using ASPEN PLUS," *Renew. Energy*, vol. 101, pp. 629–636, 2017.

[7] L. Backham, E. Croiset, and P. L. Douglas, "Simulation of a coal hydrogasification process with integrated CO2 capture BT - Greenhouse Gas Control Technologies 7," no. 519, pp. 1941–1945, 2005.

[8] M. Fernandez-Lopez, J. Pedroche, J. L. Valverde, and L. Sanchez-Silva, "Simulation of the gasification of animal wastes in a dual gasifier using Aspen Plusï¿½," *Energy Convers. Manag.*, vol. 140, pp. 211–217, 2017.

[9] H. J. Jeong, D. K. Seo, and J. Hwang, "CFD modeling for coal size effect on coal gasification in a two-stage commercial entrained-bed gasifier with an improved char gasification model," *Appl. Energy*, vol. 123, pp. 29–36, 2014.

[10] G. Li *et al.*, "Application of general regression neural network to model a novel integrated fluidized bed gasifier," *Int. J. Hydrogen Energy*, vol. 43, no. 11, pp. 5512–5521, Mar. 2018.

[11] N. Lerkkasemsan, "Fuzzy logic-based predictive model for biomass pyrolysis," *Appl. Energy*, vol. 185, pp. 1019–1030, Jan. 2017.

[12] M. J. V. A. SARRIA BIENVENIDO, "Análisis comparativo de las características fisicoquímicas de la cascarilla de arroz.," *Sci. Tech.*, no. 37, p. 6, 2007.

[13] W. C. Yan *et al.*, "Model-based downdraft biomass gasifier operation and design for synthetic gas production," *J. Clean. Prod.*, vol. 178, pp. 476–493, 2018.

[14] P. Breeze and P. Breeze, "Advanced Waste-to-Energy Technologies," in *Energy from Waste*, Elsevier, 2018, pp. 65–75.

[15] R. C. Saxena, D. Seal, S. Kumar, and H. B. Goyal, "Thermo-chemical routes for hydrogen rich gas from biomass: A review," *Renew. Sustain. Energy Rev.*, vol. 12, no. 7, pp. 1909–1927, 2008.

[16] C. . Guerrero, F. . Sierra, and S. Ramirez, "Gasification technology of the organic materials," *Proc. XIX Int. Mater. Res. Congr.*, p. 145, 2010.

[17] V. Kirubakaran, V. Sivaramakrishnan, R. Nalini, T. Sekar, M. Premalatha, and P. Subramanian, "A review on gasification of biomass," *Renew. Sustain. Energy Rev.*, vol. 13, no. 1, pp. 179–186, 2009.

[18] X. T. Li, J. R. Grace, C. J. Lim, A. P. Watkinson, H. P. Chen, and J. R. Kim, "Biomass gasification in a circulating fluidized bed," *Biomass and Bioenergy*, vol. 26, no. 2, pp. 171–193, 2004.

[19] S. R. Rubio, F. E. Sierra, and A. Guerrero, "Gasificación de materiales orgáni- cos residuales Gasification from waste organic materials," *Ing. e Investig.*, vol. 31, no. 3, pp. 17–25, 2011.